Radiometric calibration of DJI Mavic 3M multispectral images: a comparison of automatic processing, empirical line method, and field spectroradiometer

Matheus Modesto da Silva [1], Rebeca Campos Emiliano da Silva [2], Antonio Maria Garcia Tommaselli [3], Nilton Nobuhiro Imai [4]

[1] Department of Cartography, São Paulo State University (UNESP) at Presidente Prudente, São Paulo, Brazil – (matheus.modesto, rebeca.campos, a.tommaselli, nilton.imai)@unesp.br

Keywords: Radiometric calibration, Mavic 3M, Empirical Line Method, Spectroradiometer, Multispectral images.

1. Introduction

Radiometric calibration is a fundamental task in remote sensing for many applications. The aim of radiometric calibration is to reduce some effects associated with the radiance recorded by the sensor system, such as atmospheric conditions and lighting geometry, preserving the radiometric properties of the targets and enabling the extraction of quantitative values expressed in physical units (Smith and Milton, 1999). The empirical line method (ELM) is commonly used to obtain the surface reflectance from an optical image (Farrand et al., 1994). The ELM assumes that within an image, for any spectral band (λ), there is one or more homogeneous targets of light and dark colours, whose reflectances are known and can be determined in the field with a spectroradiometer. A simple linear regression is then applied using the digital numbers (DNs) of these targets and their respective reflectances to estimate the coefficients of the equation (Ben-Dor et al., 1994; Moran et al., 2001).

Research on radiometric calibration by ELM often highlights the importance of the quantity of radiometric targets used in the linear regression, as well as the physical characteristics and colours of these materials. These factors are essential for improving the precision of the model and the accuracy of predicting the reflectance of the target of interest, as demonstrated by Ben-Dor et al. (1995) and Farrand et al. (1994).

The commercial development of compact Unmanned Aerial Vehicles (UAVs) equipped with multispectral sensors integrated with positioning systems (Global Navigation Satellite System (GNSS) receivers with Inertial Measurement Unit (IMU) and auxiliary sensors, such as the sunlight sensor on the DJI Mavic 3M, has gained importance due to their ease of operation, cost-effectiveness and data quality. Sunlight sensors integrated into UAVs, capable of measuring solar irradiance, represent a simplified alternative for obtaining data in physical units of reflectance or radiance (Daniels et al., 2023). The manufacturer states that the Mavic 3M solar sensor is located on the top of the equipment and measures solar irradiance in real time (DJI, 2024). These measurements assist in the radiometric adjustment of the image, helping to maximise the precision of the multispectral data collected. Additionally, the integration of this data is compatible with most of the photogrammetric processing software, which simplifies the radiometric calibration workflow. However, many of these tools are operated by users with limited technical training, limiting their ability to critically assess the radiometric quality of the products generated (Cao et al., 2019; Pajares, 2015).

Considering these techniques, it is necessary to investigate whether the automatic method of radiometric calibration of multispectral images based on a sunlight sensor is suitable for quantitative analysis, comparing it with existing techniques and with field data acquired with a spectroradiometer. Therefore, this work compares three sets of reflectance data: (i) the orthomosaics generated from the automatic calibration based on information from the sunlight sensor of the DJI Mavic 3M UAV; (ii) the orthomosaic calibrated using the ELM; and (iii) the reflectance values obtained in the field with the ASD FieldSpec spectroradiometer. The comparison aims to assess the radiometric accuracy of the calibration methods applied to multispectral images.

2. Methodology

2.1 Study area and data acquisition

The experiment was conducted at the Faculty of Science and Technology – UNESP campus, located in the municipality of Presidente Prudente, state of São Paulo, Brazil (22°07’19.94’’ S, 51°24’28.54’’ O). The multispectral images were acquired by the 1/2.8-inch CMOS (Complementary Metal-Oxide-Semiconductor) sensor (Table 1) on board the DJI Mavic 3M drone, operating in the spectral bands of Green (560 nm), Red (650 nm), RedEdge (730 nm) and NIR (860 nm, Near InfraRed). The flight campaign took place on June 5, 2025, at a flight height of 100 meters, with frontal and lateral overlap of 80% and 60%, respectively. In addition, to ensure precise positioning of the camera's exposure stations, an RTK base (DJI D-RTK 2) was used throughout the operation.

Sensor details	Specifications
Field of view (FOV)	73.91° (61.2° × 48.10°)
Focal length	4.34 mm
Aperture	f/2.0
Type of focus	Fixed
Shutter speed	Electronic: 1/30 ~ 1/12.800 s
Pixel size	1.998 µm
Image size	2592 × 1944 pixels
Image format	TIFF

Table 1. Technical characteristics of the DJI Mavic 3M Sensor.

Ten radiometric targets with different physical properties and grey tones were positioned in the study area. Six of them are made of medium-density fibreboard (MDF) (measuring 50 × 50 cm), painted with acrylic tints in different concentrations, ranging from black to white. These tints included the special Musou Black paint (Koyo Orient Japan co., LTD.), with a high light absorption rate (99.4%). The remaining four targets are made of ethylene-vinyl-acetate (EVA) (measuring 45 × 45 cm), with shades of black, light grey, dark grey and white. In addition, a natural vegetation target was identified and measured. The spectral profile of each target was acquired *in situ* using an ASD FieldSpec HandHeld spectroradiometer with a 1° lens.

2.2 Geometric processing

The geometric processing of the multispectral images was carried out using the commercial software Agisoft Metashape, version 2.1.2 (Agisoft LLC, 2022). The project parameters were defined with an initial precision of 20 cm for the camera position components (X, Y, Z) and 2° for the rotation angles (ω, φ, k). The reference system adopted was the SIRGAS2000, with UTM projection, zone 22 South. The ground control was composed of six ground control points (GCPs) and two check points (CPs), which were surveyed with a precision of 9 mm for planimetry and 15 mm for altimetry. The photogrammetric processing of the image block was performed with the following workflow: (1) initial alignment in an arbitrary system, resulting in a sparse point cloud; (2) measurement of the GCPs for the bundle block adjustment, imposing constraints from the flight trajectory and GCPs; (3) automatic and manual filtering of the point cloud to remove outliers; (4) optimization of the camera's interior orientation parameters (IOPs); (5) generation of a dense point cloud from the sparse cloud and the correspondence between points in the images; (6) generation of the Digital Terrain Model (DTM) and orthomosaic. Then, the orthomosaics of each spectral band were exported with a Ground Sample Distance (GSD) of 4.6 cm.

2.3 Radiometric processing

To obtain the three sets of reflectance data, the multispectral orthomosaics were radiometrically processed using two different approaches. First, the automatic radiometric calibration was performed in the Metashape software, enabling the "*Use sun sensor*" tool. During the procedure, the software automatically extracts the metadata from each multispectral image, which includes information from the optical sensor and reading values acquired by the sunlight sensor integrated into the UAV. The software uses this data to estimate internal corrections for each pixel, based on the ratio between the light reflected by the target and the incident light at the instant the images were captured. Subsequently, an orthomosaic is generated for each spectral band, and the pixel values must be divided by 32.768 (2^{15}) to obtain the normalised apparent reflectance values.

The spectral radiance measurements obtained in the field by the spectroradiometer were converted into a reflectance factor. This conversion considered the radiance reflected by both the target of interest (L_T) and the reference plate (L_r) (Spectralon plate), within the same wavelength range, in addition to the application of a correction factor (k), defined as the ratio between the solar irradiance and the reference plate's radiance (Jensen, 2009).

$$\rho_T = \frac{L_T}{L_r} \cdot k \qquad (1)$$

Subsequently, a band simulation was performed for the optical sensor, as it measures not only the central wavelength, but a weighted average value based on its bandwidth. Therefore, the reflectance factor obtained from the spectroradiometer is adjusted to reproduce the sensor's integrated spectral response within each band.

In the second approach, radiometric calibration using an ELM was carried out through a manual workflow using the Microsoft Excel spreadsheet editor and QGIS software, version 3.34.35 (QGIS Development Team, 2023). The steps in QGIS consisted of: (1) normalization of the orthomosaics; (2) subtraction of a black level constant (Dark Current); (3) creation of a shapefile with the delimitation of the 11 radiometric targets, each with a 5 × 5 pixel dimension (equivalent to 23 × 23 cm, considering a GSD of 4.6 cm); (4) extraction of statistical values - sum, mean, minimum, maximum, variance and standard deviation - of the DNs of each corresponding polygon, for each spectral band, using the "*Zonal Statistics*" tool. To calculate the slope (a) and intercept (b) coefficients of the linear regression equation, an Excel spreadsheet was organised containing the average DNs of the radiometric targets (Figure 1) together with their respective field reflectances, used to adjust the linear model (Iqbal et al., 2018).

$$R = a \times DN + b \qquad (2)$$

With the coefficients calculated, the linear regression equation was applied to the dataset using the "*Raster Calculator*" tool in QGIS software.

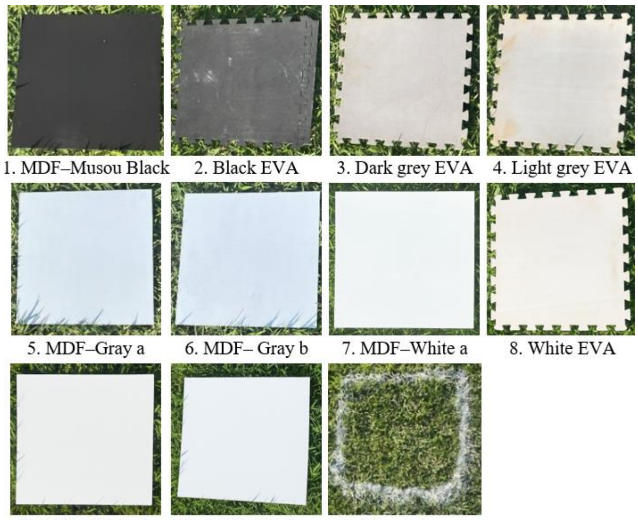

Figure 1. Radiometric targets organised and identified by their respective numbering (1 to 10).

By applying both approaches, it was possible to analyse and compare the vegetation reflectance predictions obtained through the automatic calibration of the Metashape software against the ELM, using field data as a reference.

3. Results

The results of this study, based on the application of the ELM, focused on analysing the linear fit of the model and identifying the most suitable radiometric targets for predicting vegetation reflectance across all multispectral bands. It was observed that standardising the same set of targets for all bands is unfeasible, since the exposure and their spectral properties vary according to the wavelength. The predicted vegetation reflectance for each band was compared to the reference value, which was obtained from field measurements, as a quality control.

As shown in Figure 2, the linear fit for the four multispectral bands was found by first examining all ten radiometric targets along with the target of interest. Only the targets that best fit to predict their reflectances were then shown.

It is observed, mainly in the green band, a saturation of most of the bright radiometric targets, as shown in Figure 2.a, where the targets present different reflectance values but nearly identical DN values, close to 1, in normalised scale, which corresponds to a DN of 2^{16} (65.535) for a 16 bits image.

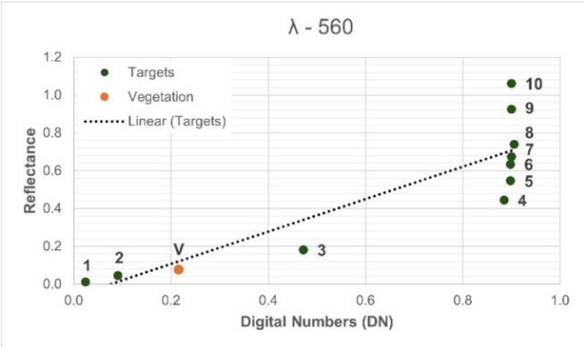

a

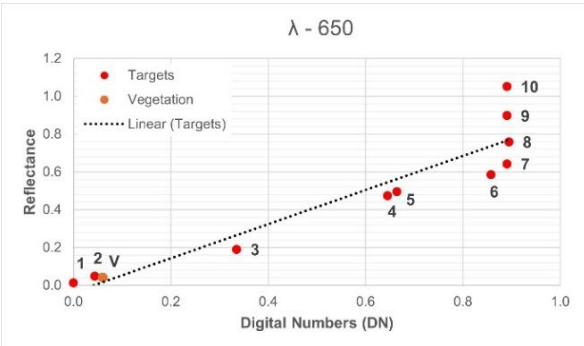

b

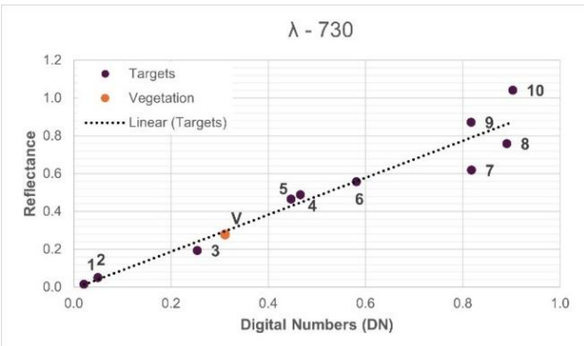

c

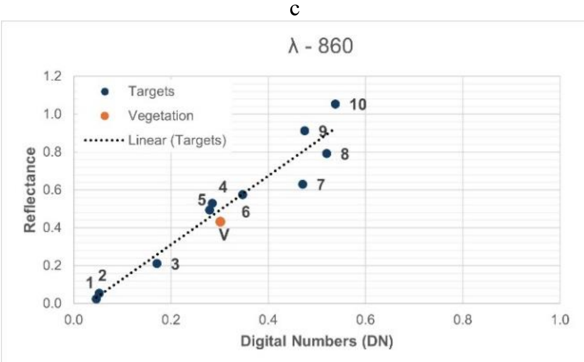

d

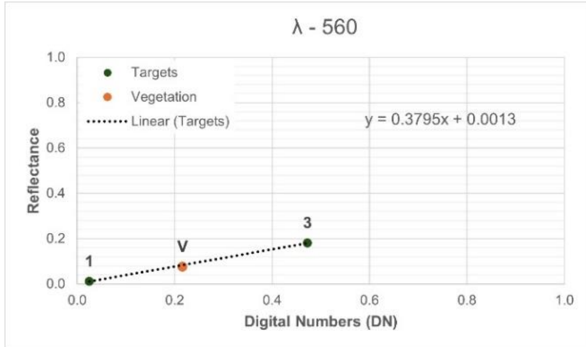

e

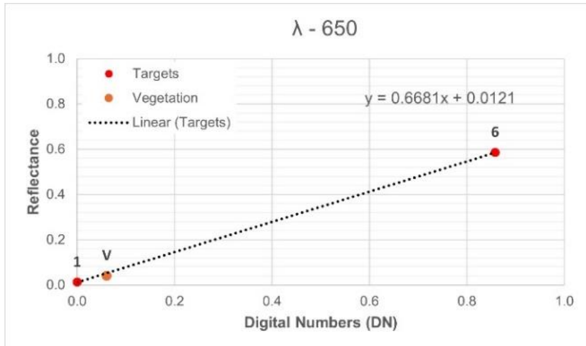

f

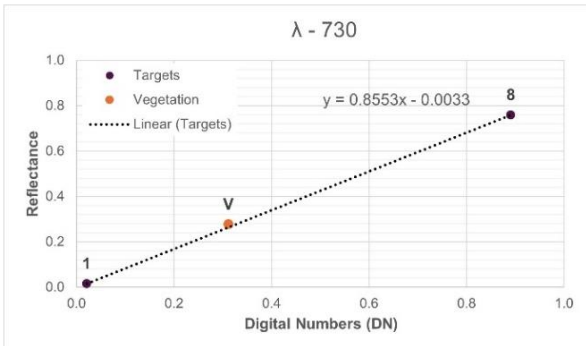

g

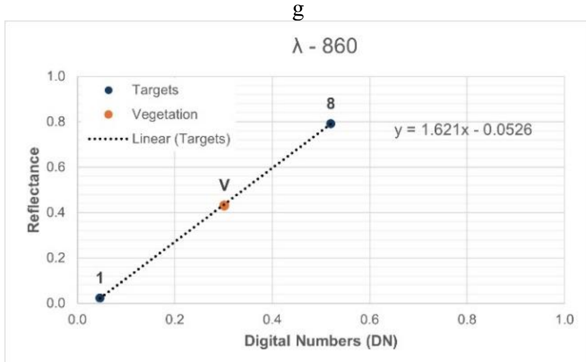

h

Figure 2. Linear adjustment for the four multispectral bands: comparison between all radiometric targets (a–d) and the two selected targets (e–h).

This phenomenon is directly related to the higher sensitivity of this band to reflected radiation. Based on the graphical analysis of the targets in each band, it was possible to select those most suitable for the linear regression. Therefore, it is evident that two targets were sufficient to cover the minimum and maximum reflectance, ensuring that the vegetation remained within the prediction limits of the model. In the analysis of the Green band, it was observed that targets 4 (EVA-Light Gray), 5 (MDF-Gray a), 6 (MDF-Gray b), 7 (MDF-White a), 8 (EVA-White), 9 (MDF-White b), and 10 (MDF-White c) exhibited evidence of saturation (Figure 2.a). Therefore, targets 1 (MDF-Musou Black) and 3 (EVA-Dark Gray) were selected for the regression (Figure 2.e).

For the Red band, the chosen targets were 1 (MDF-Musou Black) and 6 (MDF-Gray b) (Figure 2.f). For the RedEdge band, targets 1 (MDF-Musou Black) and 8 (EVA-White) were used (Figure 2.g). Regarding the NIR band, the selected targets were the same as those used for the RedEdge band (Figure 2.h). It should be noted that the MDF target painted with Musou Black exhibited the lowest reflectance in all bands, while the maximum reflectance was represented by different targets that varied based on the multispectral band analysed.

To evaluate the accuracy of vegetation reflectance prediction between the two estimation approaches, the Absolute Error (AE) metric was used. The results showed values ≤ 1% for the ELM method (AE-ELM column), while the automatic method (AE-AUT column) showed values ≥ 4%, reaching up to 13% in the NIR band, as shown in Table 2. In studies published by Xu et al. (2019) and Sun et al. (2025), errors in the range of 1–3% were observed for the prediction targets, which are considered satisfactory, indicating that the results obtained with ELM are consistent with these findings. In contrast, the automatic method presented errors higher than those reported in the literature, showing lower accuracy in estimating vegetation reflectance, for this study case.

Band	a	b	AE-ELM	%	AE-AUT	%
560	0.379	0.001	0.008	0.8	0.04	4
650	0.668	0.012	0.01	1	0.03	3
730	0.855	-0.003	0.01	1	0.08	8
860	1.621	-0.053	0.006	0.6	0.13	13

Table 2. Regression coefficients and absolute errors.

In Figure 3, the spectral signature of the target of vegetation was compared to measurements collected with the ASD and those estimated using the ELM and the automatic method (Automatic). The results obtained with the automatic method overestimated the reflectance values for all wavelengths, demonstrating its limitations. On the other hand, the ELM produced vegetation reflectance very close to the field reference, with the lines almost overlapping. Figure 4 shows the difference between the predicted and reference vegetation reflectance.

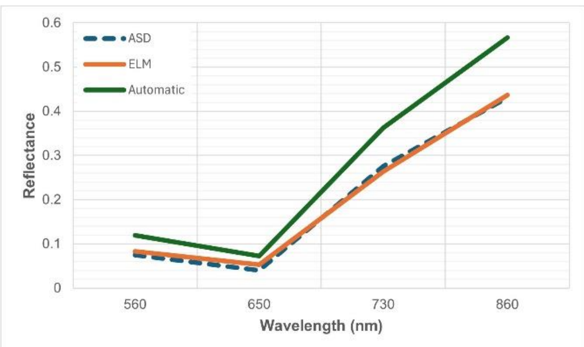

Figure 3. Spectral signature of vegetation from the three approaches.

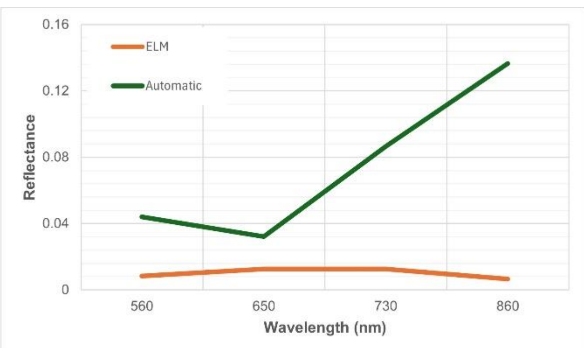

Figure 4. Difference between the predicted and the reference of vegetation reflectance values.

4. Conclusion

The results showed that the ELM method was more consistent and closer to the field reflectance, demonstrating its effectiveness for radiometric correction of UAV images. Although calibration using sunlight sensor values in Metashape, though practical, showed limitations and is unsuitable for extracting quantitative information from these bands and derived vegetation indices. For future work, it is recommended to compare it with other radiometric calibration methods and to standardize a set of radiometric targets suitable for predicting vegetation.

Acknowledgements

This study was financed in part by the São Paulo Research Foundation, FAPESP (Grants 2021/06029-7) and by the National Council for Scientific and Technological Development, CNPq (grant n. 303670/2018-5 and 136831/2024-9).

References

Smith, G. M., and Milton, E. J., 1999. The use of the empirical line method to calibrate remotely sensed data to reflectance. *International Journal of Remote Sensing*, 20(13), 2653–2662. https://doi.org/10.1080/014311699211994

Farrand, W. H., Singer, R. B., and Merényi, E., 1994. Retrieval of apparent surface reflectance from AVIRIS data: a comparison of empirical line, radiative transfer and spectral mixture methods. *Remote Sensing of Environment*, 47(3), 311–321. https://doi.org/10.1016/0034-4257(94)90099-X

Ben-Dor, E., Kruse, F. A., Lefkoff, A. B., and Banin, A., 1994. Comparison of three calibration techniques for utilization of GER 63-channel aircraft scanner data of Makhtesh Ramon, Negev, Israel. *Photogrammetric Engineering and Remote Sensing*, 60(11), 1339–1354.

Moran, M. S., Bryant, R. B., Thome, K. J., Ni, W., Nouvellon, Y., González-Dugo, M. P., Qi, J., and Clarke, T. R., 2001. A refined empirical line approach for reflectance factor retrieval from Landsat-5 TM and Landsat-7 ETM+. *Remote Sensing of Environment*, 78(1–2), 71–82. https://doi.org/10.1016/S0034-4257(01)00250-4

Daniels, L., Eeckhout, E., Wieme, J., Dejaegher, Y., Audenaert, K., and Maes, W. H., 2023. Identifying the optimal radiometric calibration method for UAV-based multispectral imaging. *Remote Sensing*, 15(11), 2909. https://doi.org/10.3390/rs15112909

Cao, S., Habib, A., and Al-Badr, A., 2019. Radiometric calibration assessments for UAS-borne multispectral sensors: a framework for operational use. *ISPRS Journal of Photogrammetry and Remote Sensing*, 155, 115–128. https://doi.org/10.1016/j.isprsjprs.2019.08.013

Pajares, G., 2015. Overview and current status of remote sensing applications based on unmanned aerial vehicles (UAVs). *Photogrammetric Engineering and Remote Sensing*, 81(4), 281–330. https://doi.org/10.14358/PERS.81.4.281

Agisoft LLC, 2022. *Agisoft Metashape* [software]. Version 2.1.2. St. Petersburg, Russia. Available at: https://www.agisoft.com/ (Accessed: 15 May 2025).

QGIS Development Team, 2023. *QGIS Geographic Information System* [software]. Open Source Geospatial Foundation. Available at: https://www.qgis.org (Accessed: 15 May 2025).

DJI, 2024. *Mavic 3 Multispectral* [UAS platform]. Available at: https://ag.dji.com/pt-br/mavic-3-m (Accessed: 15 May 2025).

Jensen, J. R., 2011. *Remote sensing of the environment: an Earth resource perspective*, 2nd ed., Chapter 2. São José dos Campos: Editora Parêntese.

Iqbal, F., Lucieer, A., and Barry, K., 2018. Simplified radiometric calibration for UAS-mounted multispectral sensor. *European Journal of Remote Sensing*, 51(1), 301–313. https://doi.org/10.1080/22797254.2018.1432293

Xu, K., Gong, Y., Fang, S., Wang, K., Lin, Z., & Wang, F., 2019. Radiometric calibration of UAV remote sensing image with spectral angle constraint. *Remote Sensing*, 11(11), 1291. https://doi.org/10.3390/rs11111291

Sun, H., Guo, L., & Zhang, Y., 2025. Accurate conversion of land surface reflectance for drone-based multispectral remote sensing images using a solar radiation component separation approach. *Sensors*, 25(8), 2604. https://doi.org/10.3390/s25082604